applied optics

Smooth end face termination of microstructured, graded-index, and step-index polymer optical fibers

Ricardo Oliveira,* Lúcia Bilro, and Rogério Nogueira

Instituto de Telecomunicações, Pólo de Aveiro, 3810-193 Aveiro, Portugal
**Corresponding author: oliveiraricas@av.it.pt*

Received 26 December 2014; revised 29 April 2015; accepted 21 May 2015; posted 26 May 2015 (Doc. ID 231176); published 12 June 2015

A new technique, based on a partially automated process, for smooth end face termination of three types of plastic optical fibers (microstructured, graded-index, and step-index) is presented. The cross-sectional shape of the fibers is preserved, and the structure in microstructured plastic optical fibers (POFs) is of good quality, showing no plastic deformations. The termination is achieved in a fast and easy way, independent of material properties or structures inside the fiber. The process is reproducible and it shows that thin-diameter POFs can be used. The POFs' near-field pattern and the insertion loss are also analyzed, showing good coupling capabilities.

OCIS codes: (060.2340) Fiber optics components; (060.4005) Microstructured fibers; (160.5470) Polymers; (240.5450) Polishing; (240.6700) Surfaces.

http://dx.doi.org/10.1364/AO.54.005629

1. INTRODUCTION

In recent years, polymer optical fibers (POFs) have been regarded as a viable alternative to silica fibers in many fields [1–5]. In fact, POFs are mainly composed of polymethylmethacrylate (PMMA), a material with a Young's modulus 30 times lower than silica and with a higher thermo-optic coefficient [6]. Additionally, PMMA has biological compatibility [7] and high water sorption capabilities [8]. These advantages are attractive, especially the Young's modulus in which large strains can be imposed in POFs without breaking the fiber [1].

Initially, POF development was focused in step-index POF (SI-POF). Since then, other fiber structures were created to provide new properties. One of them is the microstructured POF (mPOF), a porous fiber, created with different geometries that can be designed to give some specific properties, such as an endlessly single-mode, air-guiding operation, and the ability to expose the electric field of the guided mode to substances contained within the holes [2]. Another interesting type of POF is the graded-index POF (GI-POF). This fiber is composed of an amorphous perfluorinated polymer (commercially known as CYTOP), and it is regarded as the best choice for high data transmission rates [3]. The main advantages of this POF are the low attenuation in the near infrared and infrared regions, together with easy handling and high transmission bandwidth, making it a low cost alternative to traditional glass fibers in home networks.

It is well known that the POFs' end face quality is one of the main challenges when the coupling process is needed, especially in mPOFs. Thus, the best POF end face quality must be achieved in order to avoid too much insertion loss and back reflections (i.e., return loss). For that reason, many authors have been working on this topic using different techniques, such as the semiconductor dicing (SD) saw [9], focused-ion-beam (FIB) milling [9], ultraviolet (UV) laser cleaving [9,10], hot blade cleaving [11–13], the connectorization process [14–16], and, more recently, the liquid nitrogen cleaving method [17].

Among these different techniques, the most popular is hot blade cleaving, where a dedicated device is used to cut the fiber. In this method different parameters are taken into account, such as the temperature, velocity and quality of the razor blade, as well as the temperature of the base where the fiber is placed [11–13]. Thus, different materials/dopants, microstructures, and even the speed in which the fiber is pulled down on the drawing process [18] will impose a combination of different parameters for each kind of fiber, leading to a time consuming process.

What is concerning about the techniques that use the SD saw, FIB milling, and the UV and liquid nitrogen cleaving methods is that they tend to be a viable process in the laboratory but not in the field. Additionally, the fiber diameter reported on those works only cover values higher than 400 μm, which is high when compared with some of the fibers commercially available in the market (>100 μm).

The connectorization process is thought to be one of the best choices for the POFs' end face termination. With this method, the POF can be glued into a ferrule of a connector

and polished, simplifying the coupling process. However, in this method, the authors agree that the fiber core concentricity is not perfectly aligned to the center of the connector ferrule [14]. That core misalignment is due to the pre-etching of the fiber, with regard to fill the bore of the ferrule [14,15], or can be due to the use of a larger bore ferrule when compared to the POF [16]. In fact, this process presents some problems that can compromise the efficiency of the technique. This is not only because of the concentricity of the fiber inside the bore of the ferrule but is also due to the concentricity of the core related to the fiber. This last factor plays an important role for POFs, since current manufacturing processes do not follow standard procedures, leading to fluctuations in concentricity and even in the dimensions of the structures along the fiber length. For multimode (MM) POFs, the coupling using the connectorization process is not a concern because the core is too large. On other hand, when the fiber is single-mode (SM), the process can be challenging [15]. In addition, the current polishing processes were totally made by hand which can introduce imperfections from the user.

In this work, we show a new methodology to produce a smooth POF end face termination. It is based on a dual step procedure with a hot blade cleaving together with a commercial device dedicated for end face termination of silica optical fiber connectors. The process is fast, reliable, and semi-automatic, avoiding human errors and offering unprecedented end face quality. The prepared POFs are well suited for applications regarding free-space coupling to other POFs or silica pigtail fibers, solving problems related with the concentricity of the core in POFs. Finally, to prove the good quality of the results and knowing that most of the optical equipment such as sources and detectors are based on silica fiber, it was made as a free-space coupling between a silica pigtail fiber and the different POFs prepared. In that way, the insertion loss measurements of each coupling were provided. The near-field pattern used to assist the coupling is also shown, revealing good coupling results.

2. POFS' END FACE PREPARATION

The proposed methodology was validated for three fiber types, specifically: mPOF, SI-POF, and GI-POF. The fibers are composed of different material types, where the mPOFs (except the SM-340 and the FM with Rh6G) are totally composed of PMMA. For the SM-340 mPOF, an outer polycarbonate (PC) layer covers the microstructured PMMA structure. In what concerns the FM with Rh6G, the PMMA material is doped with Rhodamine 6G. For the SI fibers the material is essentially PMMA, where the SM-MORPOF03 has a core doped with 5% of polystyrene (PS), and the MM-MORPOF01 has a fluorinated cladding. For the GI-POF, the material that composes the inner part of the fiber is a perfluorinated polymer and the outer region is composed of PC. The detailed specifications of the fibers used in this work can be seen in Table 1.

To begin the POFs' end face preparation, a hot blade was used to first cleave the fiber, avoiding crack formation in the transversal and longitudinal directions, and allowing at the same time the formation of a flat surface. The blade used has a "v"-shaped edge, with 200 μm thickness and 1000 μm height. The cutting process was handmade with the fibers laid onto a piece of glass and cleaved transversally to the POF. The base was left at room temperature, while the blade temperature was set to cleave the fibers without melting or creating cracks. That temperature was set to be below the melting point of PMMA and CYTOP materials (around 70°C or 80°C). After the cleaving process, the POFs were analyzed with an optical fiber scope (OFS300-200C) to check if any visible crack was formed. If so, the process is repeated with higher temperatures. After the cleaving process, the fibers were subjected to a polishing procedure with a connector polishing machine (REV Connector Polisher, from Krell Technologies). Ferrules of physical contact connectors (FC-PC) with 2.5 mm external diameter were used to fill the support of the FC-PC connector machine.

It is known that the POFs' external diameter fluctuates through its length [19]. In some types of fibers, these diameters may fluctuate around 10 μm or even more. Therefore, the ferrules inner hole (bore) was selected to cover different diameters ranging from 80 to 640 μm. After selecting the specific ferrule that closely matches the POF being used, the cleaved POF is inserted in the ferrule bore and pulled down against the polishing machine film. The polishing process takes two cycles with 15 s duration time. The first cycle is made with a 3 μm grain size (PF03.0S-P-2) polishing film and the second one with 0.3 μm (PF00.XW-P-2). The grain sizes of the polishing films were chosen to first roughly scratch the POFs' end face, removing imperfections from the hot blade process and the second one to give a smooth termination. To avoid small dust particles in the end face of the fiber, specifically for the mPOFs, water spray was spread onto the second polishing film prior to the polishing step.

3. POFS' END FACE QUALITY ANALYSIS

The quality of the POFs' end face was numerically analyzed by the measurement of different variables present on the microscope fiber images. For that, different machine vision tools from National Instruments-Vision Builder software were used.

Table 1. POF Specifications

POF Fiber	Company	Type	Hole d (μm)	Hole Layers	Cladd D (μm)	Core d (μm)
FM-250	Kiriama	mPOF	3.2	6	250	18
FM w/Rh6G	Kiriama	mPOF	–	4	180	11
G3-250	Kiriama	mPOF	–	3	250	34
MM-150	Kiriama	mPOF	3.5	3	150	40
SM-340	Kiriama	mPOF	3.9	6	340	8
SM-125	Kiriama	mPOF	1.4	6	125	4
GI-POF	Chromis Fiberoptics	GI	–	–	500	50
SM-MORPOF03	Paradigm Optics	SI	–	–	125	8
MM-MORPOF01	Paradigm Optics	SI	–	–	250	240

Those images were selected to contain all structures as well as enough resolution for an accurate detection and measurement. The selected variables were: the cladding diameter and its ellipticity, defined as the ratio between the major and minor orthogonal diameters, where a value near the unit reveals a circular shape; the core diameter as well as the core ellipticity, in the case of the SI-POFs; the core shift, calculated through the difference between the center of the cladding circular edge, and the mean center of the hole structures for mPOFs as well as the center of the core in case of the SI-POFs; and finally, the mPOFs' mean hole diameter, together with its mean ellipticity.

4. INSERTION LOSS MEASUREMENTS

The insertion loss measurements were done using short pieces of POFs terminated on each side by the previously reported process. The method was based on a single-ended measurement, with a laser source operating at 850 nm, a reference pigtail silica fiber, and an optical power meter. The reference power was measured with the pigtail silica fiber, where the FC/APC connector was coupled to the source, and the end terminal of the pigtail was cleaved at 90° and inserted into a 125 μm FC/PC bare fiber adaptor, following the attachment to the power meter. After measuring the reference power, the short pieces of POFs were butt coupled to the silica pigtail fiber. A video camera with 3× magnification was used to help the alignment and control the distance between the two fibers. At the same time, the near-field pattern of the POFs' end face was collected by a laser beam profiler (LBP2-VIS) through a 40× microscope objective. This process was seen in real time in order to precisely align the beam into the POF core.

Finally, the POF terminal is inserted in a ferrule bore with suited dimensions for each POF and connected to the power meter. The insertion loss (CL) was calculated taking into account the reference power (RP), the measured total loss (TL), the length of the POF (L), and the known fiber loss (FL), following the equation: $CL = RP - TL - (L * FL)$.

5. RESULTS

The results for the POFs' end face preparation are shown in Fig. 1. It can be seen that the POFs' shape appears to be preserved, as well as the air holes in the case of mPOFs. It is also shown that the fiber's end face appears with no cracks.

After acquiring the POFs' tip microscope images, a precise and quantitative numerical investigation was performed. For that, the automated machine vision tools were employed on the images and the corresponding structure parameters were collected. The POFs' optical microscope images together with all vision machine tools used are shown in Fig. 2.

After a proper fit of the vision tools, all the data were collected and can be seen in Table 2.

The presented values for the cladding, core, and mean hole diameters are in accordance with the ones presented in Table 1. The small fluctuations between them, which are related to the presently immature manufacturing process, lead to fluctuations in the fiber parameters through its length. In terms of the data obtained for ellipticity of the cladding, core, and holes in case of mPOFs, the values were all equal to one, except for the holes for the G3-250 fiber, where their shape is already defined to be

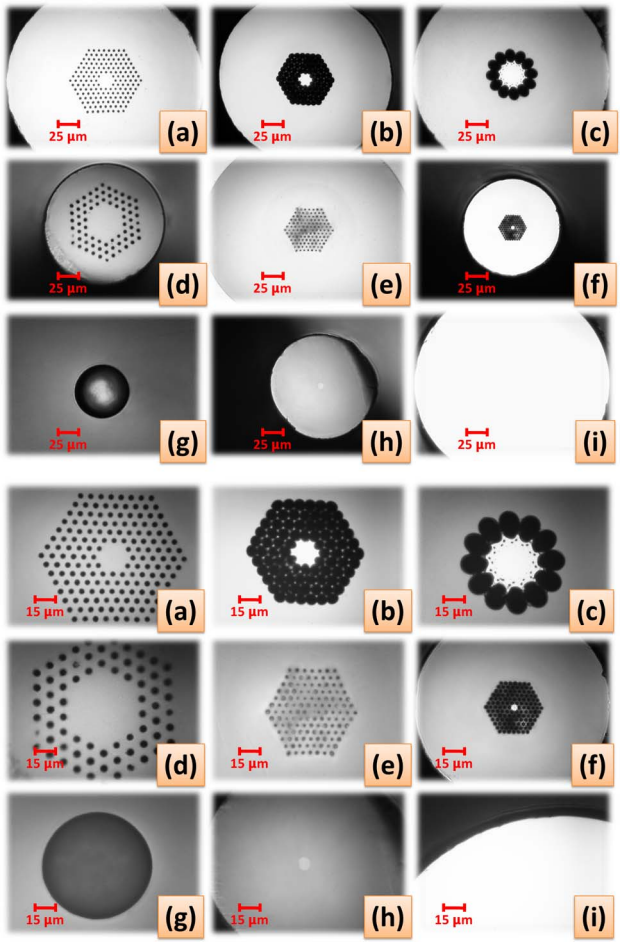

Fig. 1. Optical microscope images of several POFs with different structures and sizes, for two different magnification lenses (M) (M = 10 × for the upper images, and M = 20 × for the lower images). The letters refer to (a) mPOF FM-250; (b) mPOF FM with Rh6G; (c) mPOF G3-250; (d) mPOF MM-150; (e) mPOF SM-340; (f) mPOF SM-125; (g) GI-POF (the GI-POF end face images only cover the fiber core); (h) SM-MORPOF03; and (i) MM-MORPOF01 [the lower MM-MORPOF01 image only shows a small portion of the fiber (core–cladding–air)].

elliptical. For the core shift, the values were below 1 μm except for the SM-MORPOF03 and GI-POF, which had in the worst case 1.3 μm. It should be noted that the results presented here may contain small deviations due to the distortions of the acquired images as well as the inherent errors from the detection software. In the overall analysis it can be concluded that the results are of high quality. Additionally, the core POFs are centered, which avoids constraints related with the core shift that are associated with the hot blade cleaving method [13]. This reveals that the first polishing procedure removes a great amount of the POF terminal and inherently the defects associated with the initial hot blade cleaving process. The near-field images collected prior to the insertion loss measurements are shown in Fig. 3. It is shown that light injected from the silica pigtail fiber into the POFs can be strongly coupled to the core (see Fig. 3, right-hand side), revealing the integrity of the core mode's shape.

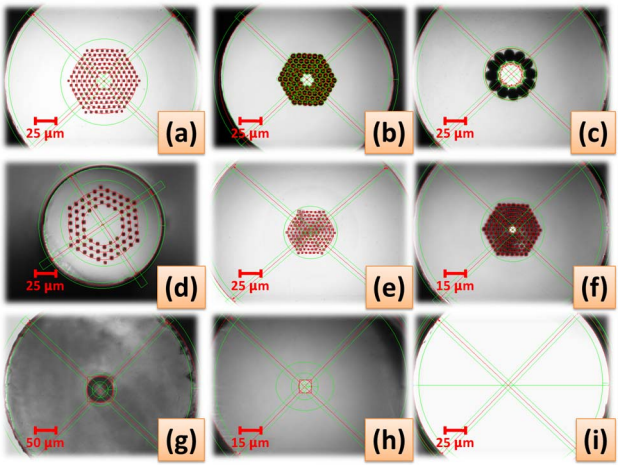

Fig. 2. POFs' optical microscope images after the introduction of different vision tools for (a) mPOF FM-250; (b) mPOF FM with Rh6G; (c) mPOF G3-250; (d) mPOF MM-150; (e) mPOF SM-340; (f) mPOF SM-125; (g) GI-POF; (h) SM-MORPOF03; and (i) MM-MORPOF01. The magnification lens of the microscope images was 5× for (g); 10× for (f) and (h); 20× for (a), (b), (c), (d), (e), and (i).

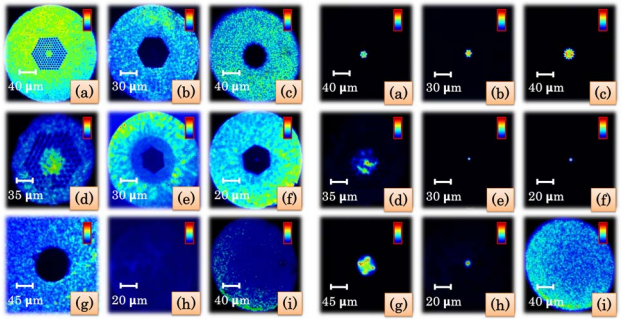

Fig. 3. POFs' near-field images, before (left) and after (right) the free-space coupling to a pigtail silica fiber. The letters refer to (a) mPOF FM-250; (b) mPOF FM with Rh6G; (c) mPOF G3-250; (d) mPOF MM-150; (e) mPOF SM-340; (f) mPOF SM-125; (g) GI-POF (due the large diameter POF, only the inner part of this fiber is shown); (h) SI SM-MORPOF03; and (i) SI MM-MORPOF01.

Table 3 shows the measured insertion losses when the prepared polished fibers are used with free-space coupling to a silica pigtail fiber.

The measured values for the insertion loss are different for each fiber type. The main reason is related to the difference between the core size of the pigtail silica fibers (9 or 50 μm), related to the POFs' core. Results show that the insertion loss is higher when the silica core fiber is greater than that of the POF, as predicted. Thus, the coupling of the SM-125 POF presented the highest insertion loss, because part of the light injected by the 9 μm silica core cannot enter into the 4 μm mPOF. The same explanation is used for the SM-340 fiber, but since the core diameter mismatch is smaller, the insertion loss is also smaller. On the other hand, when the silica fiber has a lower core diameter than the POF, the insertion loss obtained is lower (e.g., for the couplings made with FM-250, FM with Rh6G, G3-250, and MM-MORPOF01).

In the MM-150 fiber, we made two tests with different pigtail silica core sizes (9 and 50 μm). As predicted, the higher loss values were obtained when the silica core was higher than the POF. Comparing the values it can be noted that there are almost 4 dB difference between the two couplings made, which in some way compromises the connection from the 50 μm core silica fiber to the 40 μm POF core. Additionally, the higher insertion loss values attained for this POF have inherent loss contributions from the weak mode distribution around the MM mPOF core, as seen in Fig. 3(d), right-hand side. This weak mode distribution is related to the short length of mPOF used (only 38 cm), which imposes additional losses.

The insertion loss obtained for the GI-POF was the best one, achieving 0.13 dB. This value is reflected in part of the perfect core matching, and also in the perfect smooth end face provided by the polishing process. For the SM-MORPOF03, the total loss is indeed high. Without knowing the manufactured fiber loss, we can say that part of that high loss is due to the doped materials present in the POF, as well as the smaller fiber core (8 μm), related to the silica pigtail (9 μm).

Nevertheless, it should be noted that the values presented here for the insertion loss of the different polished POFs are inherently subjected to the free-space coupling made, meaning that the silica fiber to POF coupling may have some angular misalignments between them, as well as refractive index mismatching.

Table 2. POFs' End Face Numerical Analysis

POF Fiber	Cladd d (μm)	Cladd Ellipt.	Core d (μm)	Core Ellipt.	Core Shift (μm)	Mean Holes d (μm)	Mean Holes Ellipt.
FM-250	249.5	1.0	19.9	–	0.5	3.3	1.0
FM w/Rh6G	190.8	1.0	11.3	–	0.4	5.7	1.0
G3-250	289.3	1.0	28.6	–	1	19.8 &14.8	1.3
MM-150	143.4	1.0	43.9	–	0.6	4.0	1.0
SM-340	340.6	1.0	9.7	–	0.5	3.5	1.0
SM-125	122.7	1.0	3.8	–	0.4	1.6	1.0
GI-POF	491.8	1.0	63.9	1.0	1.1	–	–
SM-MORPOF03	134.4	1.0	8.3	1.0	1.3	–	–
MM-MORPOF01	254.4	1.0	239.7	1.0	0.6	–	–

Table 3. Insertion Loss Measurements at 850 nm

POFs	L (cm)	Silica-POF core (μm)	Loss (dB/m)	Total Loss (dB)	Insertion Loss (dB)
FM-250	30	9 → 18	2	1.90	1.30
FM w/Rh6G	40	9 → 11	3	2.04	0.84
G3-250	15	9 → 34	1,5	1.86	1.64
MM-150	38	9 → 40	2	6.00	<5.40
MM-150	38	50 → 40	2	9.40	<8.64
SM-340	13	9 → 8	2.5	2.30	1.98
SM-125	20	9 → 4	6	7.50	6.30
GI-POF	28	50 → 50	0.06	0.15	0.13
SM-MORPOF03	10	9 → 8	–	6.50	<6.50
MM-MORPOF01	33	50 → 240	3.5	1.62	0.47

6. CONCLUSION

The POF end face termination presented is capable in producing cross sections with high quality without compromising the integrity of the POFs' outer shape or the microstructure (if present). Problems associated with crack formation or core-shift presented by other methods were easily solved by the polishing process. The time consumption for the entire process, including cleaving and polishing, takes about 1 min. To the best of the authors' knowledge, this is a significant improvement considering the current state-of-art techniques. The process works for different POF diameters, even for thin fibers as the ones presented in this work (i.e., 125 μm) and it is partially automated, avoiding imperfections from the technician, making the process easy and repeatable. The fibers terminated with this process were tested in a free-space coupling with silica fibers, revealing a good performance. The ability to obtain POFs' end face with high quality, as those presented in this work, will result in better performances in POF-based systems, such as those for sensors and communications.

Fundação para a Ciência e a Tecnologia (Portuguese Science and Technology Foundation) (PTDC/EEATEL/122792/2010), (PEst- OE/EEI/LA0008/2013), (SFRH/BD/88472/2012), (SFRH/BPD/78205/2011).

REFERENCES

1. Z. Xiong, G. D. Peng, B. Wu, and P. L. Chu, "Highly tunable Bragg gratings in single-mode polymer optical fibers," IEEE Photon. Technol. Lett. **11**, 352–354 (1999).
2. M. C. J. Large, D. Blacket, and C. A. Bunge, "Microstructured polymer optical fibers compared to conventional POF: novel properties and applications," IEEE Sens. J. **10**, 1213–1217 (2010).
3. Y. Shao, R. Cao, Y.-K. Huang, P. N. Ji, and S. Zhang, "112-Gb/s transmission over 100 m of graded-index plastic optical fiber for optical data center applications," in *Optical Fiber Communication Conference* (Optical Society of America, 2012), paper OW3J.5.
4. C. A. F. Marques, L. Bilro, N. J. Alberto, D. J. Webb, and R. Nogueira, "Narrow bandwidth Bragg gratings imprinted in polymer optical fibers for different spectral windows," Opt. Commun. **307**, 57–61 (2013).
5. S. Liehr, P. Lenke, M. Wendt, K. Krebber, M. Seeger, E. Thiele, G. Gebreselassie, and J. C. Munich, "Polymer optical fiber sensors for distributed strain measurement and application in structural health monitoring," IEEE Sens. J. **9**, 1330–1338 (2009).
6. M. C. J. Large, L. Poladian, G. Barton, and A. v. E. Martijn, *Microstructured Polymer Optical Fibres* (Springer, 2007).
7. C. Markos, W. Yuan, K. Vlachos, G. E. Town, and O. Bang, "Label-free biosensing with high sensitivity in dual-core microstructured polymer optical fibers," Opt. Express **19**, 7790–7798 (2011).
8. O. Rodríguez, F. Fornasiero, A. Arce, C. J. Radke, and J. M. Prausnitz, "Solubilities and diffusivities of water vapor in poly(methyl-methacrylate), poly(2-hydroxyethylmethacrylate), poly(N-vinyl-2-pyrrolidone) and poly(acrylonitrile)," Polymer **44**, 6323–6333 (2003).
9. S. Atakaramians, K. Cook, H. Ebendorff-Heidepriem, V. Afshar, J. Canning, D. Abbott, and T. M. Monro, "Cleaving of extremely porous polymer fibers," IEEE Photon. J. **1**, 286–292 (2009).
10. J. Canning, E. Buckley, N. Groothoff, B. Luther-Davies, and J. Zagari, "UV laser cleaving of air–polymer structured fibre," Opt. Commun. **202**, 139–143 (2002).
11. O. Abdi, K. C. Wong, T. Hassan, K. J. Peters, and M. J. Kowalsky, "Cleaving of solid single mode polymer optical fiber for strain sensor applications," Opt. Commun. **282**, 856–861 (2009).
12. S. H. Law, J. D. Harvey, R. J. Kruhlak, M. Song, E. Wu, G. W. Barton, M. A. van Eijkelenborg, and M. C. J. Large, "Cleaving of microstructured polymer optical fibres," Opt. Commun. **258**, 193–202 (2006).
13. A. Stefani, K. Nielsen, H. K. Rasmussen, and O. Bang, "Cleaving of TOPAS and PMMA microstructured polymer optical fibers: core-shift and statistical quality optimization," Opt. Commun. **285**, 1825–1833 (2012).
14. A. Abang and D. J. Webb, "Demountable connection for polymer optical fiber grating sensors," Opt. Eng. **51**, 080503 (2012).
15. A. Abang, D. Saez-Rodriguez, K. Nielsen, O. Bang, and D. J. Webb, "Connectorization of fibre Bragg grating sensors recorded in microstructured polymer optical fibre," Proc. SPIE **8794**, 87943Q (2013).
16. R. Lwin and A. Argyros, "Connecting microstructured polymer optical fibres to the world," presented at the International Conference on Plastic Optical Fibers, Sydney, Australia, 7–11 September 2009.
17. M. V. P. Ghirghi, V. Minkovich, and A. G. Villegas, "Polymer optical fiber termination with use of liquid nitrogen," IEEE Photon. Technol. Lett. **26**, 516–519 (2014).
18. C. Jiang, M. G. Kuzyk, J.-L. Ding, W. E. Johns, and D. J. Welker, "Fabrication and mechanical behavior of dye-doped polymer optical fiber," J. Appl. Phys. **92**, 4–12 (2002).
19. G. Barton, M. A. van Eijkelenborg, G. Henry, M. C. J. Large, and J. Zagari, "Fabrication of microstructured polymer optical fibres," Opt. Fiber Technol. **10**, 325–335 (2004).